MATERIALS CHEMISTRY
FRONTIERS

RESEARCH ARTICLE

View Article Online
View Journal | View Issue

Cite this: *Mater. Chem. Front.*, 2023, 7, 5431

Deep-red/NIR AIEgens based on electron-withdrawing dithiafulvalene-fused benzothiadiazole for solution-processed non-doped OLEDs†

Yanling Liu,‡[a] Ziwei Deng,‡[a] Jiale Li,[b] Jianlong Xie,[b] Xing Feng,[c] Zijie Qiu,[a] Guohua Xie,*[b] Zheng Zhao*[ad] and Ben Zhong Tang*[ae]

Received 26th May 2023,
Accepted 28th August 2023

DOI: 10.1039/d3qm00598d

rsc.li/frontiers-materials

Deep-red (DR)/near-infrared (NIR) emitters have extensive applications in bioimaging and flexible optoelectronics. However, it is challenging to design efficient DR/NIR emitters with high photoluminescence quantum yields (PLQYs), especially in the solid state, due to the energy gap law. A common strategy to develop new acceptors is to construct donor–acceptor luminogens with fine-tuned molecular structures. Nevertheless, new acceptors that are suitable for constructing highly efficient DR/NIR emitters are still rare. Herein, by utilizing cyano-substituted dithiafulvalene fused benzothiadiazole (BSMCN) as the acceptor and triphenylamine derivatives as donors, three BSMCN-based molecules, respectively, named 2TB, 2MTB, and 2MOTB, are rationally designed and efficiently synthesized. All three compounds exhibit aggregation-induced emission properties with their emission wavelengths extending from the DR to NIR region. Moreover, when applied in solution-processed non-doped devices, 2TB exhibits a high external quantum efficiency of 4.9% at a wavelength of 664 nm, demonstrating the great potential of BSMCN-based DR/NIR AIEgens in developing non-doped OLEDs.

Introduction

The development of highly efficient organic deep-red/near-infrared (650–900 nm) fluorescent emitters is significant due to their extensive applications in bioimaging and flexible optoelectronics,[1–7] but also a challenging task due to the limit of the energy-gap law.[8–10] Indeed, with the decrease of the band gap (corresponding to long emission wavelengths), the quenching factors like vibrational coupling, twisted intramolecular charge transfer, and conical intersection are more likely to occur, which boost the non-radiative decay channels and quench the emission.[11]

Construction of donor–acceptor (D–A) structures is the most commonly used strategy to generate DR/NIR luminogens because the band gap of the D–A compounds could be greatly narrowed in comparison with both the D and A moieties due to the reorganization of the orbitals of D and A.[12,13] There are abundant donor moieties to choose, such as aromatic amines, thiophene derivatives, fulvene, *etc.* However, acceptors with the strong electron-withdrawing capability are still limited. The commonly used benzothiadiazole (BT), pyridal[2,1,3]thiadiazole (PT), and benzobis(thiadiazole) (BBT) either show a weak electron-withdrawing ability or are difficult to prepare or purify, which inspire the development of new acceptors.[14–19] Recently, cyano-substituted dithiafulvalene fused benzothiadiazole (BSMCN) has been demonstrated as a promising acceptor for constructing new D–A semiconductors for bioimaging and organic light-emitting diode (OLED) applications.[20–22] As the acceptor contains both electron-rich sulfur and electron-withdrawing cyano groups and the benzothiadiazole moiety, its sulfur-rich property benefits the charge transport of semiconductors. Meanwhile, fusion with the electron-withdrawing group could effectively suppress the quenching effect of sulfur atoms to fluorescence, enabling the construction of highly efficient long wavelength emitters.[23]

[a] *School of Science and Engineering, Shenzhen Institute of Aggregate Science and Technology, The Chinese University of Hong Kong, Shenzhen (CUHK-SZ), Guangdong 518172, China. E-mail: zhaozheng@cuhk.edu.cn, tangbenz@cuhk.edu.cn*
[b] *Sauvage Center for Molecular Sciences, Hubei Key Lab on Organic and Polymeric Optoelectronic Materials, Department of Chemistry, Wuhan University, China. E-mail: guohua.xie@whu.edu.cn*
[c] *School of Material and Energy, Guangdong University of Technology, Guangzhou 510006, P. R. China*
[d] *HKUST Shenzhen Research Institute, Shenzhen 518057, China*
[e] *Department of Chemistry, Hong Kong Branch of Chinese National Engineering Research Center for Tissue Restoration and Reconstruction, The Hong Kong University of Science and Technology, 100071 Hong Kong, China*

† Electronic supplementary information (ESI) available. CCDC 2265565 and 2265566. For ESI and crystallographic data in CIF or other electronic format see DOI: https://doi.org/10.1039/d3qm00598d

‡ These authors contributed equally to this work.

However, luminogens based on BSMCN have not been well developed, and are worth further exploration.

DR/NIR OLEDs possess huge advantages for application in night-vision devices, information-secured displays, and lighting fixtures.[24–28] However, in comparison with the well-developed green and yellow light electroluminescence devices, the performances of DR/NIR OLEDs lag behind.[29–35] By employing the design principles of hybridized local and charge transfer (HLCT) and thermally activated delayed fluorescence (TADF), the limit of 25% EQE in OLED devices could be broken.[36–39] However, the design of efficient HLCT and TADF characterized DR/NIR molecules is still challenging, especially those with high PLQY. Moreover, most DR/NIR luminogens having a D–A structure easily suffer the aggregation-caused quenching (ACQ) effect due to the strong intermolecular π–π stacking resulting from the intermolecular D–A interactions.[40] Although doping organic emitters with host materials may solve the ACQ problem to some extent, the doping concentration needs to be precisely controlled to decrease the emission quenching and suppress the roll-off effect caused by exciton annihilation.[41] Moreover, the doped film may also suffer the drawbacks of high-cost mass production and phase separation, resulting in performance degradation upon heating and technological complexity because of the addition of dopants.[42,43] Thus, it is highly desirable to develop luminogens that are suitable for non-doped devices. In terms of this, luminogens with aggregated-induced emission (AIE) characteristics provide a much more suitable choice since they exhibit much more enhanced emission upon aggregation.

In this work, by utilizing BSMCN as the acceptor and triphenylamine derivatives as donors, three BSMCN-based molecules named 2TB, 2MTB, and 2MOTB were designed and efficiently synthesized. All three molecules exhibited typical aggregation-induced emission (AIE) properties with the emission maximum ranging from 691 nm to 749 nm and high PLQY in the solid state. In particular, 2TB exhibited a high PLQY of 33.4%. Based on the superior PL properties of these luminogens, we further prepared non-doped electroluminescent (EL) devices based on them. Among them, the EL device based on 2TB exhibited a quite high EQE of 4.9% at a wavelength of 664 nm, and those based on 2MTB also exhibited a high EQE of 3.6% at a wavelength of 690 nm. These results indicate that BSMCN-based DR/NIR emitters are promising candidates for high-performance non-doped OLED devices.

Results and discussion

Synthesis and characterization

The synthetic routes for 2TB, 2MTB, and 2MOTB are presented in Scheme 1, while the targeting molecules could be efficiently obtained in two steps with high yields. Firstly, the intermediates M1, M2, and M3 could be obtained by Suzuki coupling of 4,7-dibromo-5,6-difluorobenzo[*c*][1,2,5]thiadiazole and boronic acid of TPA derivatives with yields of 83%, 77% and 84%, respectively. Then, S_NAr reactions between sodium 2,2-dicyanoethene-1,1-bis(thiolate) and intermediates M1, M2, and M3 in the presence of

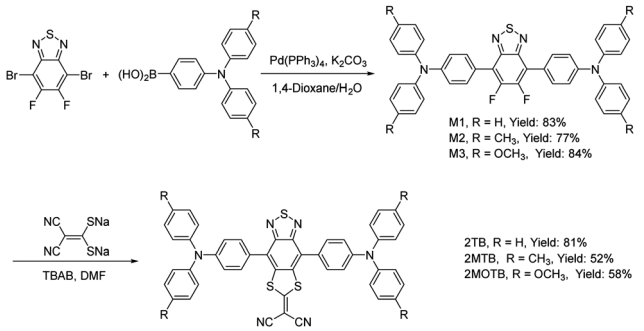

Scheme 1 The synthetic routes for 2TB, 2MTB, and 2MOTB.

tetrabutylammonium bromide (TBAB) afforded the targeting molecules of 2TB, 2MTB, and 2MOTB with yields of 81%, 52%, and 58%, respectively. All the targeting compounds and intermediates were fully characterized by ^{1}H NMR, ^{13}C NMR, and high-resolution mass spectroscopy (HRMS) (Fig. S1–S12, ESI†).

Photophysical properties and theoretical calculations

The optical properties of the target molecules were investigated and are shown in Fig. 1 and Table S1 (ESI†). The three molecules showed similar UV-vis absorption spectra with three peaks at around 330, 390, and 480 nm, respectively. The two peaks at shorter wavelengths were ascribed to the locally excited (LE) transition, while the longer one was associated with the intramolecular charge transfer (ICT) absorption from the TPA segments to the BSMCN moiety (Fig. 1a).[44] Furthermore, the absorption of LE and CT states was well consistent with the D–A structure.[45,46] All three molecules showed bright emission in the solid state with emission maximums at 691, 702, and 749 nm, respectively, demonstrating that BSMCN is a good acceptor to afford DR/NIR emitters (Fig. 1b).[47] With the enhancement of the electron donating ability (H < CH_3 < OCH_3), the emission showed a trend of redshift, suggesting enhanced intramolecular charge transfer. Besides, the solvatochromic effect investigation indicated that, with the solvent polarity increase, the emission intensity of 2TB and 2MTB gradually decreased and their emission wavelengths exhibited obvious redshift, suggesting that both 2TB and 2MTB display twisted intramolecular charge transfer (TICT) (Fig. S13, ESI†),[48] while for 2MOTB no emission was observed in polar solvents due to its too strong TICT effect.[49] The TICT effect matches well with the PL properties of the three molecules since the TICT effect is responsible for both the long wavelength emission and low PLQY. The relatively weak emission in common organic solvents like THF and strong emission in the solid state suggest the AIE activity of the three molecules. We thus investigated the AIE behavior of the three molecules. As shown in Fig. 1c, the PL intensity of 2TB in THF solution exhibits maximum emission at 677 nm. With increasing the water fraction (f_w) in the THF solution of 2TB from 0% to 50%, the emissions were gradually quenched due to the TICT effect. Further increasing the f_w from 60% to 90%, the emission was greatly enhanced (Fig. 1d). 2MTB exhibited similar AIE behavior to 2TB (Fig. S14, ESI†).

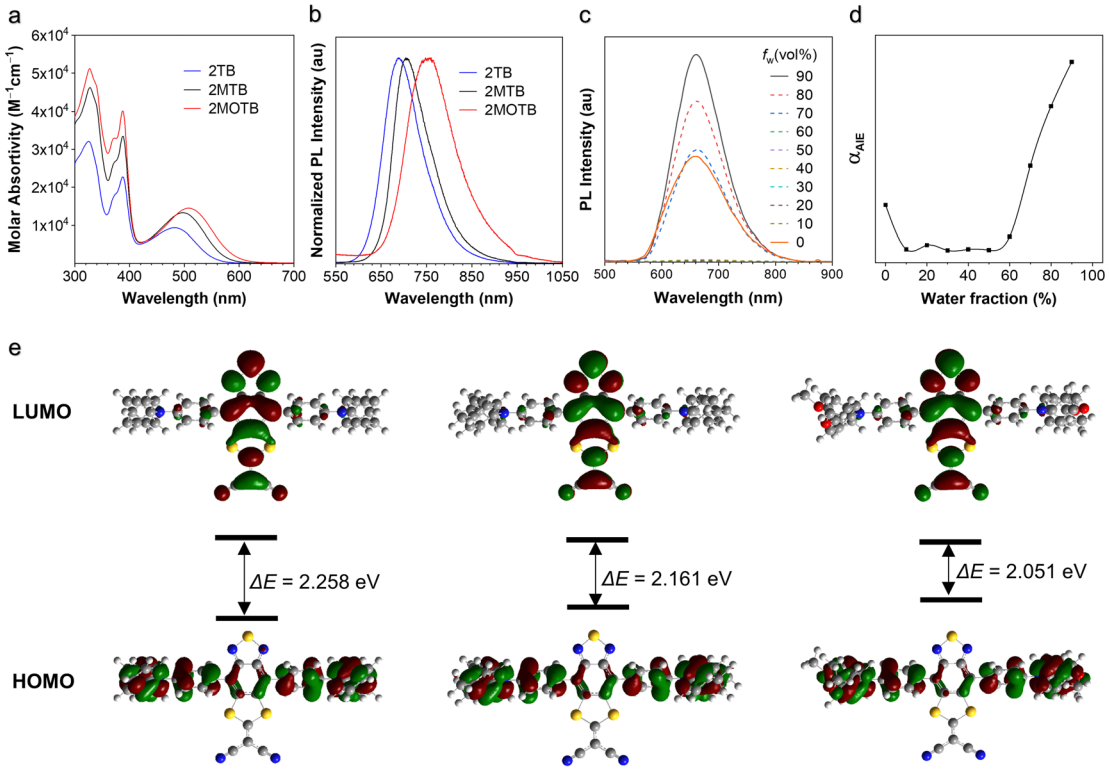

Fig. 1 The optical spectra of 2TB, 2MTB, and 2MOTB. (a) UV-vis spectra of 2TB (blue), 2MTB (black), and 2MOTB (red) in THF. (b) PL spectra of 2TB (blue), 2MTB (black), and 2MOTB (red) films. (c) PL intensity of 2TB in THF/water mixtures; f_w (vol %) is the volume fraction of water; concentration = 10 μM. (d) Plot of the α_{AIE} of 2TB *versus* different f_w, where $\alpha_{AIE} = I/I_0$, with I_0 being the PL intensity in pure THF. (e) Calculated HOMOs and LUMOs of 2TB, 2MTB and 2MOTB in the ground state by DFT at the B3LYP/6-31g(d,p) level.

Interestingly, unlike the solid-state emission showing a redshift from the emission in solution, the emission wavelengths of aggregates (in the THF/water mixture, and the fraction of water is 90%) of 2TB (661 nm) and 2MTB (680 nm) exhibited blueshifts compared to the solution (Table S1, ESI†). The blueshift of the emission wavelength of aggregates from that of solution suggested that the aggregation-induced rigidification prohibited the excited state conformation relaxation and thus caused the blueshift,[43] while in the solid state, stronger intermolecular interactions might form which resulted in further energy level splitting and redshift of the emission. There is still no obvious emission for aggregates of 2MOTB, which should be ascribed to the too strong TICT effect. As for 2MOTB, the THF solution is non-emissive with a PLQY of only 0.2%, while the solid exhibited a PLQY of 4.5%, demonstrating AIE activity. In addition, the transient lifetimes of 2TB, 2MTB, and 2MOTB in the solid state are within the nanosecond scale, indicating these materials lack TADF properties (Fig. S15, ESI†). The PLQYs of the three compounds are summarized in Table S1 (ESI†). Furthermore, the PLQYs of the three compounds were measured as 23.3%, 6.3%, and 0.2% for 2TB, 2MTB, and 2MOTB in THF, respectively, while the PLQYs of the films of the three compounds were measured as 33.4%, 11.9%, and 4.5%, respectively, which further support the AIE activity of the three compounds.

To better understand the optical behaviour of the three compounds, density functional theory (DFT) calculations were carried out at the B3LYP/6-31g(d,p) level (Fig. 1e).[50] In general, for the three molecules, the electron cloud density distribution of the highest occupied molecular orbitals (HOMOs) was located across the whole molecular backbone, suggesting the good conjugation of the D and A moieties, while the electron cloud density distribution of the lowest occupied molecular orbitals (LUMOs) was mainly located on the central acceptor moiety. The HOMO and LUMO electron density distributions matched well with the charge transfer properties of the three molecules. Moreover, the energy gaps of the three molecules were calculated as 2.258 eV, 2.161 eV, and 2.051 eV for 2TB, 2MTB and 2MOTB, respectively, which were also consistent with the gradually enhanced TICT effect. In addition, based on the optimized structures, the natural transition orbitals (NTO) of 2TB and 2MTB were calculated at the wB97X-D3 level using the def2-TZVP basis set which revealed that the holes were delocalized on the TPA units and BSMCN cores, while the particles were mainly localized on the central acceptor units (Fig. S17, ESI†).[51] Therefore, the transition of 2TB and 2MTB exhibited a hybrid LE and CT transition, which to some extent reduced the TICT effect and is in accordance with their obvious emission in THF solution.

Single crystal X-ray diffraction

Single crystal structures could provide a lot of information to interpret the luminescence behavior in the aggregate state. Through the solvent diffusion method with the DCM/*n*-hexane

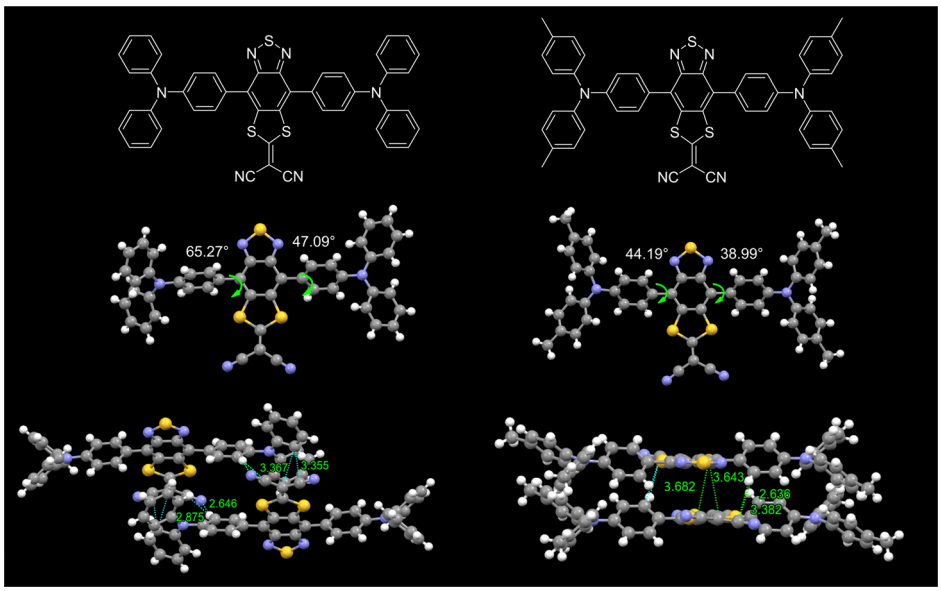

Fig. 2 The single crystal structures and packing modes of 2TB and 2MTB.

system (1/5, v/v) at ambient temperature, single crystals of 2TB and 2MTB that were suitable for crystal structure analysis were successfully obtained (Fig. 2 and SI 3.8, ESI†). Both 2TB and 2MTB exhibited twisted molecular configurations with comparable torsion angles between the acceptor and adjacent phenyl ring of the donor (47.09° and 65.27° for 2TB, 44.19° and 38.99° for 2MTB), which not only favored the emission wavelength redshift but also effectively avoided π–π stacking-induced emission quenching. Moreover, the packing mode of 2TB indicated that the molecules within the 2TB crystal exhibited no strong π–

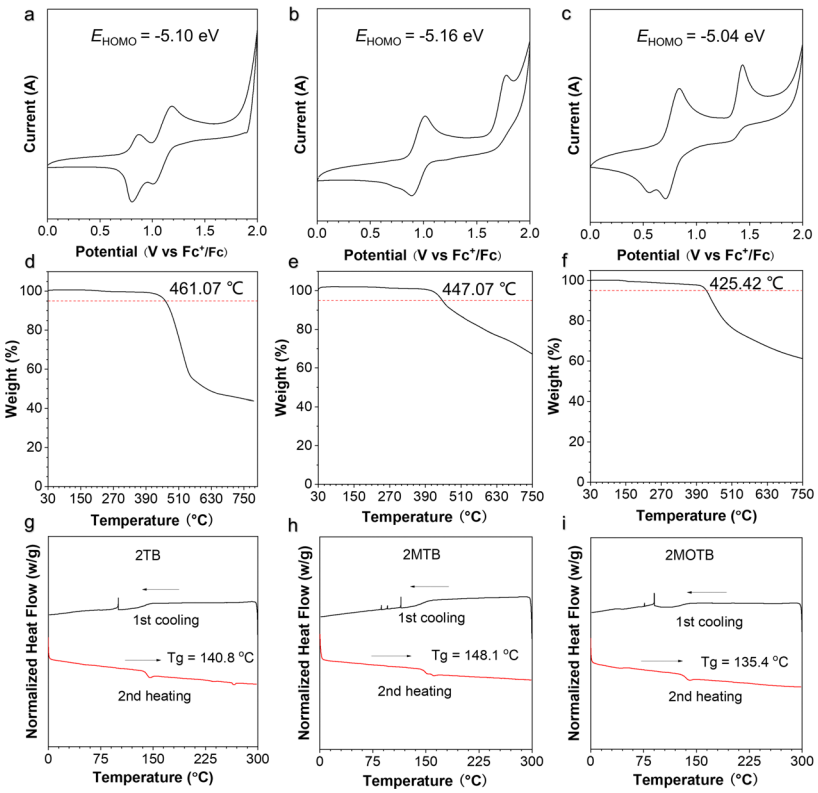

Fig. 3 The cyclic voltammetry curves of 2TB (a), 2MTB (b), and 2MOTB (c) measured in DCM with 0.1 M $BuN_4^+PF_6^-$ as the electrolyte at a scan rate of 50 mV s^{-1}. TGA curves of 2TB (d), 2MTB (e), and 2MOTB (f) under a nitrogen atmosphere at a heating rate of 20 °C min^{-1}; DSC curves of 2TB (g), 2MTB (h) and 2MOTB (i) under a nitrogen atmosphere at a heating rate of 20 °C min^{-1}.

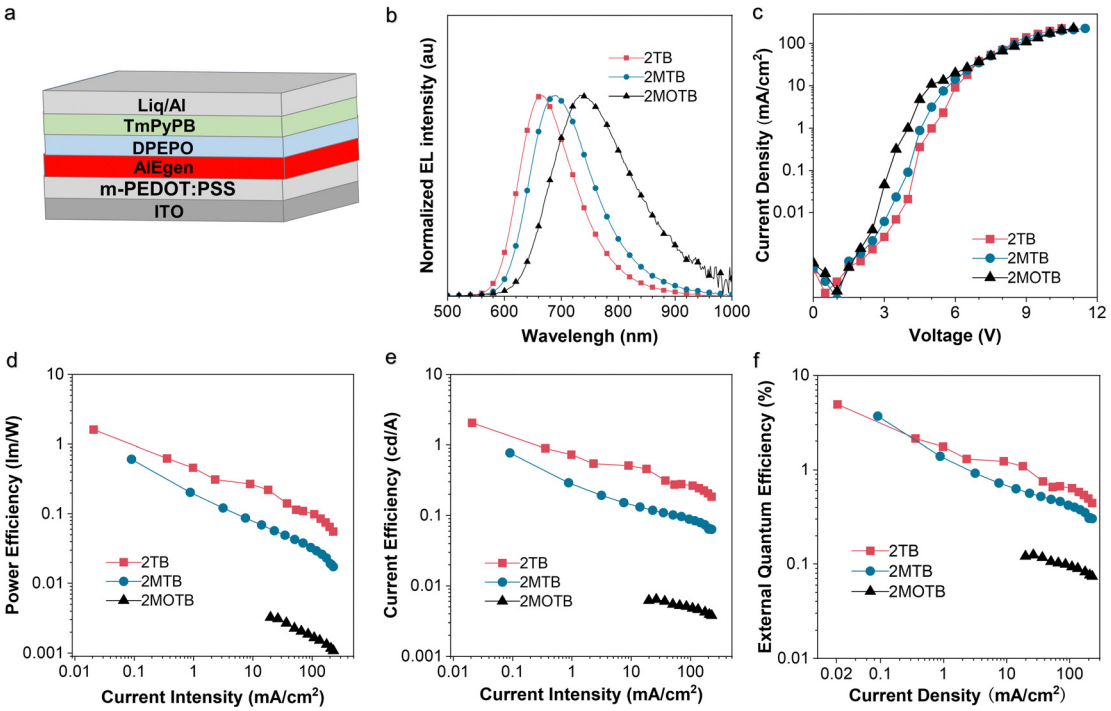

Fig. 4 (a) Schematic of the device structure of the non-doped OLEDs. (b) Normalized electroluminescence (EL) spectra of the devices based on 2TB, 2MTB, and 2MOTB. (c) Current density–voltage characteristics. (d) power efficiency, (e) current efficiency, and (f) EQE *versus* current density curves of the devices.

π stacking but multiple intermolecular C–H···π interactions which were favorable for efficient solid-state emission. As a comparison, 2MTB showed relatively closer packing with an S···π distance of 3.6–3.7 Å between the intermolecular acceptor units. The relatively strong intermolecular interaction may correlate with the lower PLQY of 2MTB.

Electrochemical and thermodynamic properties

Energy levels and thermodynamic properties are significant parameters for device fabrication. Cyclic voltammetry (CV) measurements were conducted to evaluate the energy level distribution of the three compounds. As shown in Fig. 3, 2BT exhibited two reversible oxidation waves, 2MBT exhibited one reversible oxidation wave, and 2MOBT exhibited two oxidation waves with poor reversibility. The first half-wave reductive potentials were measured as 0.76 V, 0.82 V, and 0.68 V for 2BT, 2MBT, and 2MOBT, respectively. Therefore, the HOMO energy levels of 2BT, 2MBT, and 2MOBT were calculated as −5.10 eV, −5.16 eV, and −5.04 eV, respectively, suggesting they were typical p-type semiconductors (Fig. 3a–c).[52] By integrating with optical band gaps, the LUMOs of 2BT, 2MBT, and 2MOBT were calculated as −2.92 eV, −3.11 eV, and −3.06 eV. The suitable energy levels of HOMOs and LUMOs favor both electron and hole transport. The thermodynamic properties of the three compounds were investigated by thermogravimetric analysis (TGA) and differential scanning calorimetry (DSC). TGA results indicated that the decomposition temperatures of all three compounds at a 5% weight loss were over 425 °C (Fig. 3d–f), indicating their excellent thermal stability for vacuum evaporation. Furthermore, DSC results indicated that the three AIEgens show no obvious phase change below 135 °C (Fig. 3g–i), which could effectively avoid the phase change resulting in device performance fluctuations.

OLED performance

OLEDs with the targeting AIEgen as the non-doped emissive layer were fabricated through a solution processing method with the configuration of ITO/m-PEDOT:PSS (70 nm)/AIEgens (40 nm)/DPEPO (10 nm)/TmPyPB (50 nm/Liq (1 nm)/Al (100 nm). Aluminum (Al) and indium tin oxide (ITO) acted as the cathode and anode, respectively. The modified poly(3,4-ethylenedioxythiophene)–poly(styrenesulfonate) (m-PEDOT:PSS) and lithium quinolate (Lq) served as the hole injection layer and the electron injection layer. Bis[2-(diphenylphosphino)phenyl]-ether oxide (DPEPO) functioned as the electron transport layer and hole blocking layer. 1,3,5-Tris(3-pyridyl-3-phenyl)benzene (TmPyPB) served as the electron transport layer. SEM was carried out and the images are shown in Fig. S17 (ESI†). Overall, uniform films were observed for devices based on the three compounds, suggesting the good film-forming properties of the three compounds. The device performances are shown in Fig. 4b–f. As shown in the normalized EL spectra (Fig. 4b), in general, the AIEgen based devices exhibited DR to NIR emissions peaking at 664, 690, and 734 nm, respectively. The Commission Internationale de L'Eclairage (CIE) chromaticity coordinates are (0.67, 0.32) for 2TB, (0.68, 0.31) for 2MTB, and (0.67, 0.32) for 2MOTB. Additionally, the current density–voltage curve and current efficiency, power efficiency, and EQE *versus* current density

characteristics are plotted in Fig. 4c–f, respectively. The overall EL performances are summarized in Table S2 (ESI†). In general, the solution-processed non-doped device based on 2TB exhibited the best EQE with a turn-on voltage of 4.9 V and a high EQE of 4.9% at 664 nm, which was approaching the upper limit of the fluorescent OLEDs. The solution-processed non-doped device based on 2MTB exhibited a decent EQE of 3.6% peaking at 690 nm.

However, it is worth noting the efficiency roll-off is obvious, which might be ascribed to Joule heating.[53–55] And generally, an obvious Joule heating effect was caused by the non-radiative recombination and the large current density generally. Therefore, further improving the PLQY and weakening the intermolecular interactions may help to reduce the Joule heating effect. To better understand the performance of the current molecular system, some latest molecular systems within similar wavelength regions and their maximum external quantum efficiencies (EQEmax) in non-doped pure fluorescent OLEDs were summarized (Fig. S20, ESI†).[56–59] The results indicate that BSMCN-based DR/NIR emitters are promising candidates for solution-processed non-doped OLEDs.

Conclusions

A series of efficient DR/NIR AIEgens with BSMCN as the electron acceptor and TPAs as electron donors were designed and prepared. All three molecules exhibit typical AIE properties with their emission maximums covering the DR to NIR region in the solid state. In particular, 2TB exhibited a high PLQY of 33.4%, peaking at a wavelength of 691 nm. Based on the superior PL properties of these luminogens in the solid state, non-doped electroluminescent devices based on them were evaluated through the solution-processing method. Among them, the device based on 2TB exhibited a reasonably high EQE of 4.9%, peaking at a wavelength of 664 nm and that based on 2MTB also exhibited a high EQE of 3.6% at a wavelength of 690 nm. These results indicate that BSMCN-based DR/NIR emitters are promising candidates for high-performance non-doped OLEDs.

Conflicts of interest

There are no conflicts to declare.

Acknowledgements

This research work was financially supported by the NSFC (52003228 and 52273197), Shenzhen Key Laboratory of Functional Aggregate Materials (ZDSYS20211021111400001), the Science and Technology Plan of Shenzhen (JCYJ20213241346130 38, KQTD-20210811090142053, JSGG20220606141800001, and GJHZ20210-705141810031), and the Innovation and Technology Commission (ITC-CNERC14SC01). We would like to thank the Materials Characterization and Preparation Center, The Chinese University of Hong Kong, Shenzhen for experimental measurements. We are grateful to Ms Xuan Li and Ms Guimiao Liu for their help with HRMS measurement, Mr Yang Kong for the help with NMR measurement, and Ms Liangfen Peng for the help with SEM imaging. A lot of thanks to Mr Boyuan Zhou, Mr Yun Zhao, Mr Haifei Wen, Mr Zicong Zhang and Ms Dan Liu for their help. Thanks to the AIE Institute (https://www.aietech.org.cn) for providing some technical assistance.

References

1 S. Liu, J. Han, Y. Chang, W. Wang, R. Wang, Z. Wang, G. Li, D. Zhu and M. R. Bryce, AIE-active iridium(iii) complex integrated with upconversion nanoparticles for NIR-irradiated photodynamic therapy, *Chem. Commun.*, 2022, **58**, 10056–10059.
2 H. Ye, D. H. Kim, X. Chen, A. S. D. Sandanayaka, J. U. Kim, E. Zaborova, G. Canard, Y. Tsuchiya, E. Y. Choi, J. W. Wu, F. Fages, J.-L. Bredas, A. D'Aléo, J.-C. Ribierre and C. Adachi, Near-Infrared Electroluminescence and Low Threshold Amplified Spontaneous Emission above 800 nm from a Thermally Activated Delayed Fluorescent Emitter, *Chem. Mater.*, 2018, **30**, 6702–6710.
3 J. Dai, L. Yao, C. Wang, Y. Wang, F. Liu, X. Yan, P. Sun, H. Zhang, Y. Wang, J. Zhou and G. Lu, Molecular Conformation Engineering To Achieve Longer and Brighter Deep Red/Near-Infrared Emission in Crystalline State, *J. Phys. Chem. Lett.*, 2022, **13**, 4754–4761.
4 T. Fan, M. Du, X. Jia, L. Wang, Z. Yin, Y. Shu, Y. Zhang, J. Wei, D. Zhang and L. Duan, High-efficiency narrowband multi-resonance emitter fusing indolocarbazole donors for BT. 2020 red electroluminescence and ultra-long operation lifetime, *Adv. Mater.*, 2023, **35**, 2301018.
5 J. Xue, J. Xu, Q. Liang, Y. Dai, R. Wang, Y. Yi and J. Qiao, Deepening Insights into Aggregation Effect of Intermolecular Charge-Transfer Aggregates for Highly Efficient Near-Infrared Non-Doped Organic Light-Emitting Diodes over 780 nm, *Adv. Funct. Mater.*, 2023, **33**, 2301312.
6 Y. Zou, J. Hu, M. Yu, J. Miao, Z. Xie, Y. Qiu, X. Cao and C. Yang, High-Performance Narrowband Pure-Red OLEDs with External Quantum Efficiencies up to 36.1% and Ultra-low Efficiency Roll-Off, *Adv. Mater.*, 2022, **34**, 2201442.
7 H. Wen, Z. Zhang, M. Kang, H. Li, W. Xu, H. Guo, Y. Li, Y. Tan, Z. Wen, Q. Wu, J. Huang, L. Xi, K. Li, L. Wang, D. Wang and B. Z. Tang, One-for-all phototheranostics: Single component AIE dots as multi-modality theranostic agent for fluorescence-photoacoustic imaging-guided synergistic cancer therapy, *Biomaterials*, 2021, **274**, 120892.
8 E. M. Kober, J. V. Caspar, B. Patrick Sullivan and T. J. Meyer, Application of the Energy Gap Law to the Decay of Charge-Transfer Excited States, *J. Am. Chem. Soc.*, 1982, **104**, 630–632.
9 Y. Zhang, D. Zhang, T. Huang, A. J. Gillett, Y. Liu, D. Hu, L. Cui, Z. Bin, G. Li, J. Wei and L. Duan, Multi-Resonance Deep-Red Emitters with Shallow Potential-Energy Surfaces to Surpass Energy-Gap Law, *Angew. Chem., Int. Ed.*, 2021, **60**, 20498.

10 Y. Gao, M. Yao, C. Zhou, H. Liu, S.-T. Zhang and B. Yang, Deep-red electro-fluorescence based on an excimer emission with hot-exciton channels, *J. Mater. Chem. C*, 2022, **10**, 4579–4583.
11 Y. Tu, Z. Zhao, J. W. Y. Lam and B. Z. Tang, Mechanistic connotations of restriction of intramolecular motions (RIM), *Natl. Sci. Rev.*, 2021, **8**, nwaa260.
12 Y. Li, J. Yao, C. Wang, X. Zhou, Y. Xu, M. Hanif, X. Qiu, D. Hu, D. Ma and Y. Ma, Highly efficient deep-red/near-infrared D–A chromophores based on naphthothiadiazole for OLEDs applications, *Dyes Pigm.*, 2020, **173**, 107960.
13 P. Lasitha, Radical anion formation exhibiting ''turn-on'' fluorescence sensing of hydrazine using a naphthalene diimide (NDI) derivative with a donor-acceptor-donor (D–A–D) molecular structure, *Photochem. Photobiol. Sci.*, 2020, **19**, 1603–1612.
14 Q. Nie, A. Tang, Q. Guo and E. Zhou, Benzothiadiazole-based non-fullerene acceptors, *Nano Energy*, 2021, **87**, 106174.
15 C. Wang, F. Liu, Q. M. Chen, C. Y. Xiao, Y. G. Wu and W. W. Li, Benzothiadiazole-based Conjugated Polymers for Organic Solar Cells, *Chin. J. Polym. Sci.*, 2021, **39**, 525–536.
16 J. Jiang, X. Li, M. Hanif, J. Zhou, D. Hu, S. Su, Z. Xie, Y. Gao, B. Yang and Y. Ma, Pyridal[2,1,3]thiadiazole as strong electron-withdrawing and less sterically-hindered acceptor for highly efficient donor–acceptor type NIR materials, *J. Mater. Chem. C*, 2017, **5**, 11053–11058.
17 Y. Yu, Z. Yu, Z. Ma, J. Jiang and D. Hu, D–π–A–π–D-type Fluorophores based on Pyridal[2,1,3]thiadiazole acceptor with hybridized local and charge-transfer excited-state for high-efficiency OLEDs, *Dyes Pigm.*, 2022, **208**, 110868.
18 K. Ono, S. Tanaka and Y. Yamashita, Benzobis(thiadiazole)s Containing Hypervalent Sulfur Atoms: Novel Heterocycles with High Electron Affinity and Short Intermolecular Contacts between Heteroatoms, *Angew. Chem., Int. Ed. Engl.*, 1994, **33**, 1977–1979.
19 L. Wan, X. Li, C. Song, Y. He and W. Zhang, Benzobis (thiadiazole)-based small molecules as efficient electron transporting materials in perovskite solar cells, *Sol. Energy Mater. Sol. Cells*, 2019, **191**, 437–443.
20 Y. Yu, H. Xing, D. Liu, M. Zhao, H. H. Y. Sung, I. D. Williams, J. W. Lam, G. Xie, Z. Zhao and B. Z. Tang, Solution-processed AIEgen NIR OLEDs with EQE Approaching 15%, *Angew. Chem.*, 2022, **134**, e202204279.
21 Y. Yu, H. Xing, H. Park, R. Zhang, C. Peng, H. H. Y. Sung, I. D. Williams, C. Ma, K. S. Wong, S. Li, Q. Xiong, M.-H. Li, Z. Zhao and B. Z. Tang, Deep-Red Aggregation-Induced Emission Luminogen Based on Dithiofuvalene-Fused Benzothiadiazole for Lipid Droplet-Specific Imaging, *ACS Mater. Lett.*, 2022, **4**, 159–164.
22 N. Niu, Y. Yu, Z. Zhang, M. Kang, L. Wang, Z. Zhao, D. Wang and B. Z. Tang, A cell membrane-targeting AIE photosensitizer as a necroptosis inducer for boosting cancer theranostics, *Chem. Sci.*, 2022, **13**, 5929–5937.
23 X. Gao, C.-A. Di, Y. Hu, X. Yang, H. Fan, F. Zhang, Y. Liu, H. Li and D. Zhu, Core-Expanded Naphthalene Diimides Fused with 2-(1,3-Dithiol-2-Ylidene)Malonitrile Groups for High-Performance, Ambient-Stable, Solution-Processed n-Channel Organic Thin Film Transistors, *J. Am. Chem. Soc.*, 2010, **132**, 3697–3699.
24 S. Wang, H. Zhang, B. Zhang, Z. Xie and W.-Y. Wong, Towards high-power-efficiency solution-processed OLEDs: Material and device perspectives, *Mater. Sci. Eng.*, 2020, **140**, 100547.
25 Y. Zhang, Y. Wang, J. Song, J. Qu, B. Li, W. Zhu and W.-Y. Wong, Near-Infrared Emitting MaterialsNear-Infrared Emitting Materials via Harvesting Triplet Excitons: Molecular Design, Properties, and Application in Organic Light Emitting Diodes, *Adv. Opt. Mater.*, 2018, **6**, 1870070.
26 A. Zampetti, A. Minotto and F. Cacialli, Near-infrared (NIR) organic light-emitting diodes (OLEDs): challenges and opportunities, *Adv. Funct. Mater.*, 2019, **29**, 1807623.
27 Y. Xiao, H. Wang, Z. Xie, M. Shen, R. Huang, Y. Miao, G. Liu, T. Yu and W. Huang, NIR TADF emitters and OLEDs: challenges, progress, and perspectives, *Chem. Sci.*, 2022, **13**, 8906–8923.
28 X. Yang, H. Guo, X. Xu, Y. Sun, G. Zhou, W. Ma and Z. Wu, Enhancing Molecular Aggregations by Intermolecular Hydrogen Bonds to Develop Phosphorescent Emitters for High-Performance Near-Infrared OLEDs, *Adv. Sci.*, 2019, **6**, 1801930.
29 J. Fan, Y. Zhang, Y. Ma, Y. Song, L. Lin, Y. Xu and C.-K. Wang, The role of intermolecular interactions in regulating the thermally activated delayed fluorescence and charge transfer properties: a theoretical perspective, *J. Mater. Chem. C*, 2020, **8**, 8601–8612.
30 Z. Chen, H. Zhang, D. Wen, W. Wu, Q. Zeng, S. Chen and W.-Y. Wong, A simple and efficient approach toward deep-red to near-infrared-emitting iridium(iii) complexes for organic light-emitting diodes with external quantum efficiencies of over 10%, *Chem. Sci.*, 2020, **11**, 2342–2349.
31 J. Zhang, H. Ye, Y. Jin and D. Han, Recent Progress in Near-Infrared Organic Electroluminescent Materials, *Top. Curr. Chem.*, 2021, **380**, 6.
32 J. Li, Y. Ma, S. Liu, Z. Mao, Z. Chi, P.-C. Qian and W.-Y. Wong, Soft salts based on platinum(ii) complexes with high emission quantum efficiencies in the near infrared region for in vivo imaging, *Chem. Commun.*, 2020, **56**, 11681–11684.
33 H. Zhang, Y. Xu, Z. Chen, S. Chen, R. Liu and W.-Y. Wong, Iridium(III) complexes with 1-phenylisoquinoline-4-carbonitrile units for efficient NIR organic light-emitting diodes, *iScience*, 2021, **24**, 102911.
34 W. Chen and F. Song, Thermally activated delayed fluorescence molecules and their new applications aside from OLEDs, *Chin. Chem. Lett.*, 2018, **29**, 471–474.
35 X. Hu, Y. Qin, Z. Li, H. Gao, T. Gao, G. Liu, X. Dong, N. Tian, X. Gu, C.-S. Lee, P. Wang and Y. Wang, Nearly 100% exciton utilization in highly efficient red OLEDs based on dibenzothioxanthone acceptor, *Chin. Chem. Lett.*, 2022, **33**, 4645–4648.
36 G. Li, J. Pu, Z. Yang, H. Deng, Y. Liu, Z. Mao, J. Zhao, S.-J. Su and Z. Chi, High-efficiency thermally activated delayed fluorescence materials via a shamrock-shaped design

strategy to enable OLEDs with external quantum efficiency over 38%, *Aggregate*, 2023, **4**, e382.

37 G. Yang, Y. Ran, Y. Wu, M. Chen, Z. Bin and J. You, Endowing imidazole derivatives with thermally activated delayed fluorescence and aggregation-induced emission properties for highly efficient non-doped organic light-emitting diodes, *Aggregate*, 2022, **3**, e127.

38 T. Li, S. Ying, H. Zhou, R. Wang, C. Ma, M. Sun, M. Xie, Q. Sun, W. Yang and S. Xue, Highly efficient white organic light-emitting diodes based on balanced bipolar-transporting blue hybridized local charge transfer fluorophores, *Mater. Chem. Front.*, 2023, **7**, 1403–1410.

39 Y. Shen, M. Li, W. Zhao, Y. Wang, H. Lu and C. Chen, Quinoline-based TADF emitters exhibiting aggregation-induced emission for efficient non-doped organic light-emitting diodes, *Mater. Chem. Front.*, 2021, **5**, 834–842.

40 J. Luo, Z. Xie, J. W. Y. Lam, L. Cheng, H. Chen, C. Qiu, H. S. Kwok, X. Zhan, Y. Liu, D. Zhu and B. Z. Tang, Aggregation-induced emission of 1-methyl-1, 2, 3, 4, 5-pentaphenylsilole, *Chem. Commun.*, 2001, 1740–1741.

41 M. Godumala, S. Choi, M. J. Cho and D. H. Choi, Recent breakthroughs in thermally activated delayed fluorescence organic light emitting diodes containing non-doped emitting layers, *J. Mater. Chem. C*, 2019, **7**, 2172–2198.

42 Z. Xie, C. Cao, Y. Zou, X. Cao, C. Zhou, J. He, C.-S. Lee and C. Yang, Molecular Engineering Enables TADF Emitters Well Suitable for Non-Doped OLEDs with External Quantum Efficiency of Nearly 30%, *Adv. Funct. Mater.*, 2022, **32**, 2112881.

43 Z. Zhao, H. Zhang, J. W. Y. Lam and B. Z. Tang, Aggregation-Induced Emission: New Vistas at the Aggregate Level, *Angew. Chem., Int. Ed.*, 2020, **59**, 9888–9907.

44 W. W. Lee, Z. Zhao, Y. Cai, Z. Xu, Y. Yu, Y. Xiong, R. T. Kwok, Y. Chen, N. L. Leung and D. Ma, Facile access to deep red/near-infrared emissive AIEgens for efficient non-doped OLEDs, *Chem. Sci.*, 2018, **9**, 6118–6125.

45 H. Miranda-Salinas, Y.-T. Hung, Y.-S. Chen, D. Luo, H.-C. Kao, C.-H. Chang, K.-T. Wong and A. Monkman, Controlling through-space and through-bond intramolecular charge transfer in bridged D-D′-A TADF emitters, *J. Mater. Chem. C*, 2021, **9**, 8819–8833.

46 Y. Zhang, D. Zhang, T. Huang, A. J. Gillett, Y. Liu, D. Hu, L. Cui, Z. Bin, G. Li and J. Wei, Multi-Resonance Deep-Red Emitters with Shallow Potential-Energy Surfaces to Surpass Energy-Gap Law, *Angew. Chem., Int. Ed.*, 2021, **60**, 20498–20503.

47 Q. Li, J. Xu, S. Tan, Y. Dai, J. Xue and J. Qiao, Approaching 800 nm near-infrared thermally activated delay fluorescence materials via simple malononitrile condensation strategy, *Org. Electron.*, 2022, **110**, 106645.

48 D. Liu, M. Zhang, W. Tian, W. Jiang, Y. Sun, Z. Zhao and B. Z. Tang, Molecular core–shell structure design: Facilitating delayed fluorescence in aggregates toward highly efficient solution-processed OLEDs, *Aggregate*, 2022, **3**, e164.

49 Z. R. Grabowski, K. Rotkiewicz and W. Rettig, Structural changes accompanying intramolecular electron transfer: focus on twisted intramolecular charge-transfer states and structures, *Chem. Rev.*, 2003, **103**, 3899–4032.

50 M. J. Frisch, G. W. Trucks, H. B. Schlegel, G. E. Scuseria, M. A. Robb, J. R. Cheeseman, G. Scalmani, V. Barone, G. A. Petersson, H. Nakatsuji, X. Li, M. Caricato, A. V. Marenich, J. Bloino, B. G. Janesko, R. Gomperts, B. Mennucci, H. P. Hratchian, J. V. Ortiz, A. F. Izmaylov, J. L. Sonnenberg, D. Williams-Young, F. Ding, F. Lipparini, F. Egidi, J. Goings, B. Peng, A. Petrone, T. Henderson, D. Ranasinghe, V. G. Zakrzewski, J. Gao, N. Rega, G. Zheng, W. Liang, M. Hada, M. Ehara, K. Toyota, R. Fukuda, J. Hasegawa, M. Ishida, T. Nakajima, Y. Honda, O. Kitao, H. Nakai, T. Vreven, K. Throssell, J. A. Montgomery, Jr., J. E. Peralta, F. Ogliaro, M. J. Bearpark, J. J. Heyd, E. N. Brothers, K. N. Kudin, V. N. Staroverov, T. A. Keith, R. Kobayashi, J. Normand, K. Raghavachari, A. P. Rendell, J. C. Burant, S. S. Iyengar, J. Tomasi, M. Cossi, J. M. Millam, M. Klene, C. Adamo, R. Cammi, J. W. Ochterski, R. L. Martin, K. Morokuma, O. Farkas, J. B. Foresman and D. J. Fox, *Gaussian 16, Revision C.01*, Gaussian, Inc., Wallingford, CT, 2016.

51 T. Lu and F. Chen, Multiwfn: A multifunctional wavefunction analyzer, *J. Comput. Chem.*, 2012, **33**, 580–592.

52 J. Zhou, X. Yin, Z. Dong, A. Ali, Z. Song, N. Shrestha, S. S. Bista, Q. Bao, R. J. Ellingson, Y. Yan and W. Tang, Dithieno[3,2-b:2′,3′-d]pyrrole Cored p-Type Semiconductors Enabling 20% Efficiency Dopant-Free Perovskite Solar Cells, *Angew. Chem., Int. Ed.*, 2019, **58**, 13717.

53 C. Murawski, K. Leo and M. C. Gather, Efficiency Roll-Off in Organic Light-Emitting Diodes, *Adv. Mater.*, 2013, **25**, 6801–6827.

54 C. Zou, Y. Liu, D. S. Ginger and L. Y. Lin, Suppressing Efficiency Roll-Off at High Current Densities for Ultra-Bright Green Perovskite Light-Emitting Diodes, *ACS Nano*, 2020, **14**, 6076–6086.

55 L. Zhao, D. D. Astridge, W. B. Gunnarsson, Z. Xu, J. Hong, J. Scott, S. Kacmoli, K. Al Kurdi, S. Barlow, S. R. Marder, C. F. Gmachl, A. Sellinger and B. P. Rand, Thermal Properties of Polymer Hole-Transport Layers Influence the Efficiency Roll-off and Stability of Perovskite Light-Emitting Diodes, *Nano Lett.*, 2023, **23**, 4785–4792.

56 Y. Yu, X. Chao, M. Xie, Y. Zhou, C. Ma, H. Zhou, Q. Sun, Y. Pan, W. Yang and S. Xue, Novel electro-fluorescent materials with hybridized local and charge transfer (HLCT) excited state for highly efficient deep red to near-infrared OLEDs, *Dyes Pigm.*, 2023, **215**, 111306.

57 S. Kongsabay, P. Funchien, P. Chasing, T. Sudyodsuk and V. Promarak, An efficient solution-processable hybridized local and charge-transfer (HLCT)-based deep-red fluorescent emitter for simple structured non-doped OLED, *J. Lumin.*, 2022, **248**, 118921.

58 T. Sudyoadsuk, P. Chasing, T. Kaewpuang, T. Manyum, C. Chaiwai, S. Namuangruk and V. Promarak, High efficiency and low efficiency roll-off hole-transporting layer-free solution-processed fluorescent NIR-OLEDs based on oligothiophene–benzothiadiazole derivatives, *J. Mater. Chem. C*, 2020, **8**, 5045–5050.

59 X. Wang, C. Zhong, G. Xie and X. Chen, Ester-substituted thiophene-fused benzothiadiazole as a strong electron acceptor to build D–A red emitters for highly efficient solution-processed OLEDs, *J. Mater. Chem. C*, 2022, **10**, 1127–1135.

